Rational approximations in Analytic QCD

Gorazd Cvetič[1, 2, *] and Héctor E. Martínez[1, †]

[1]*Department of Physics, Universidad Técnica Federico Santa María, Valparaíso, Chile*
[2]*Center of Subatomic Studies and Scientific-Technological Center of Valparaíso, Chile*
(Dated: October 15, 2009)

[In comparison with v1, in v2 Figs.6-8 are corrected due to a programming error; analysis extended to two different IR cutoffs; Introduction rewritten; to appear in J.Phys.G.]

We consider the "modified Minimal Analytic" (mMA) coupling that involves an infrared cut to the standard MA coupling. The mMA coupling is a Stieltjes function and, as a consequence, the paradiagonal Padé approximants converge to the coupling in the entire Q^2-plane except on the time-like semiaxis below the cut. The equivalence between the narrow width approximation of the discontinuity function of the coupling, on the one hand, and this Padé (rational) approximation of the coupling, on the other hand, is shown. We approximate the analytic analogs of the higher powers of mMA coupling by rational functions in such a way that the singularity region is respected by the approximants. Several comparisons, for real and complex arguments Q^2, between the exact and approximate expressions are made and the speed of convergence is discussed. Motivated by the success of these approximants, an improvement of the mMA coupling is suggested, and possible uses in the reproduction of experimental data are discussed.

PACS numbers:

I. INTRODUCTION

In perturbative QCD (pQCD) calculations, the coupling $a(Q^2) \equiv \alpha_s(Q^2)/\pi$ shows non-physical singularities at low energy ($-q^2 \equiv Q^2 \lesssim 0.1$ GeV^2). The aim of analytic QCD (anQCD) is to give a coupling $\mathcal{A}_1(Q^2)$ which is analytic at low Q^2 (> 0) and reproduces the high energy behavior of $a(Q^2)$. Using the Cauchy theorem we can write QCD running coupling in the integral form

$$a(Q^2) = \frac{1}{\pi} \int_{\sigma=-\Lambda^2-\eta}^{\infty} d\sigma \frac{\rho_1(\sigma)}{\sigma + Q^2}, \tag{1}$$

where $\eta \to +0$ and $\rho_1(\sigma)$ is the discontinuity function of $a(Q^2)$ along the cut axis in the complex Q^2-plane at n-loop approximation given by $\rho_1^{(n-\ell.)}(\sigma) = \text{Im}[a^{(n-\ell.)}(-\sigma - i\epsilon)]$.

The Minimal Analytic (MA) procedure of Shirkov and Solovtsov [1] removes the pQCD contribution of the unphysical cut, $0 < -\sigma \leq \Lambda^2$, keeping the discontinuity elsewhere unchanged

$$\mathcal{A}_1^{(MA)}(Q^2) = \frac{1}{\pi} \int_{\sigma=0}^{\infty} d\sigma \frac{\rho_1(\sigma)}{\sigma + Q^2}. \tag{2}$$

This expression doesn't have singularities for $Q^2 > 0$ and, as required, reproduces the high energy behavior of $a(Q^2)$. In fact, $\mathcal{A}_1^{(MA)}(Q^2)$ is analytic in the entire complex plane of Q^2 with the exception of negative semiaxis, reflecting the analyticity properties of the space-like observables.

We will consider a modification to the MA coupling [1] of Eq. (2). Following Ref. [2], the lower limit of integration is increased to a certain value M_0^2 which we set to be $\sim M_\pi^2$ ($\sim 10^{-2}$-10^{-1} GeV^2). Thus, the modified MA coupling is given by the following dispersion relation:

$$\mathcal{A}_1^{(mMA)}(Q^2) = \frac{1}{\pi} \int_{M_0^2}^{\infty} d\sigma \frac{\rho_1(\sigma)}{\sigma + Q^2}. \tag{3}$$

One of the motivations for modifying the MA in this way is to include the point $Q^2 = 0$ and its vicinity in the analyticity region of $\mathcal{A}_1(Q^2)$, something reflected by analyticity properties of the space-like observables, among them

---

*Electronic address: gorazd.cvetic@usm.cl
†Electronic address: hector.martinez@usm.cl

the V-type Adler function, where the infrared (IR) cutoff M_0^2 is: $M_0^2 \sim M_\pi^2$ ($\sim \Lambda_{\rm QCD}^2$).[1] When $M_0^2 > 0$, the analytic coupling $\mathcal{A}_1$ is a Stieltjes function, with the radius R of convergence for its Taylor expansion around $Q^2 = 0$ given by $R = M_0^2$. Stieltjes functions have the attractive property that their paradiagonal Padé approximants must converge to such functions at any complex value of the argument (except on the cut) when the order index of the approximants increases. Such a behavior is not guaranteed in MA model because there $M_0^2 = 0$ and, consequently, $Q^2 = 0$ is not a point of analyticity and $\mathcal{A}_1^{(MA)}$ is not a Stieltjes function.

In this work we investigate the behavior of the coupling $\mathcal{A}_1^{(mMA)}(Q^2)$ (with $M_0^2 \sim M_\pi^2$) of the mMA model (3) and its paradiagonal Padé approximants. In Sec. II, the basic definitions of rational (Padé) approximants and of Stieltjes functions are presented. In Sec. III we demonstrate that the narrow width approximations for the discontinuity function $\rho_1(\sigma)$ of $\mathcal{A}_1^{(mMA)}$ are equivalent to approximating $\mathcal{A}_1^{(mMA)}(Q^2)$ by paradiagonal Padé approximants; we investigate the convergence of the latter approximants to the "exact" function values $\mathcal{A}_1^{(mMA)}(Q^2)$ for $Q^2 > 0$. In Sec. IV we extend our analysis to the higher power analogs $\mathcal{A}_n^{(mMA)}$ of a^n ($n \geq 2$), construct the approximants for $\mathcal{A}_n^{(mMA)}$ based on the aforementioned paradiagonal Padé approximants for $\mathcal{A}_1^{(mMA)}$ and investigate their behavior for $Q^2 > 0$. In Sec. V we investigate the behavior of the aforementioned approximants for complex values of Q^2. In Sec. VI we propose an extension (improvement) of the mMA model, motivated by the success of the narrow width approximations of the discontinuity function $\rho_1(\sigma)$ in mMA; further, we point out the prospects for applications of such simple analytic QCD models to fitting experimental data. Section VII represents the summary of our results.

II.   PADÉ APPROXIMANTS AND STIELTJES FUNCTIONS

Consider a function $f(z)$, of a complex variable z, with power expansion about the origin given by

$$f(z) \approx \sum_{n=0}^{N+M} f_n z^n. \tag{4}$$

The Padé (or: rational) approximant, $R_M^N(z)$, is defined as the rational function

$$R_M^N(z) = \frac{\sum_{n=0}^N a_n z^n}{\sum_{n=0}^M b_n z^n}, \tag{5}$$

satisfying the condition that its expansion about $z = 0$ matches $N + M + 1$ terms in the power series expansion in (4). The paradiagonal Padé R_M^{M-1} can be written (using partial fractions) in the following way:

$$R_M^{M-1}(z) = \sum_{n=1}^M \frac{d_n}{z + z_n}, \tag{6}$$

where z_n are zeros of the denominator in Eq. (5).

If the function $f(z)$ is a Stieltjes function with a finite radius of convergence $R > 0$, i.e.

$$f(z) = \frac{1}{\pi} \int_0^{1/R} d\tau \frac{g(\tau)}{1 + \tau z}, \tag{7}$$

with $g(\tau)$ a nonnegative function, thus $f(z)$ having the real coefficients of its series expansion around $z = 0$ given by

$$f_n = \frac{(-1)^n}{\pi} \int_0^{1/R} \tau^n g(\tau) d\tau, \tag{8}$$

then a strong convergence theorem in the theory of Padé approximants applies which says: in the limit $M \to \infty$, $R_M^{M+J}(z)$ ($J \geq -1$) is equal to $f(z)$, and the poles of $R_M^{M+J}(z)$ are simple poles which lie on the interval of the negative real axis given by $-\infty < z < -R$ (Ref. [3], Sections 5.2, 5.4).

In particular, when $f(z)$ is a Stieltjes function, the Padé $R_M^{M-1}(z)$ of $f(z)$ has the form (6) with $d_n > 0$ and $z_n > 0$, the poles $-z_n$ having the following ordering: $-\infty < -z_M < -z_{M-1} < \cdots < -z_1 < -R$.

---

[1] We note that M_0 is a renormalization scheme (RSch) dependent quantity, just like Λ is (e.g., Λ in V-RSch and $\overline{\rm MS}$ RSch differ); $s_0 \equiv M_0^2/\Lambda^2$ is RSch-independent. Therefore, while we expect $M_0 \sim M_\pi$, M_0 ($\Leftrightarrow s_0$) is a free parameter of the model.

III.   APPROXIMATION OF THE COUPLING BY RATIONAL FUNCTIONS

In order to establish a relationship between $\mathcal{A}_1^{(mMA)}(Q^2)$ and a Padé approximant, we first note that the modified MA coupling in Eq. (3) is a Stieltjes function, as defined in Eq. (7) by identifying: $Q^2 = z$, $\sigma = 1/\tau$ and $\rho_1(\sigma) = \tau \tilde{g}(\tau)$. It has the convergence radius M_0^2, and the series expansion about $Q^2 = 0$ given by

$$\mathcal{A}_1^{(mMA)}(Q^2) = \frac{1}{\pi} \int_0^{1/M_0^2} d\tau \frac{\tilde{g}(\tau)}{(1 + \tau Q^2)} = \sum_{n=0}^{\infty} \tilde{L}_n (Q^2)^n, \tag{9}$$

where

$$\tilde{L}_n = \frac{(-1)^n}{\pi} \int_0^{1/M_0^2} \tau^n \tilde{g}(\tau) d\tau, \tag{10}$$

and $\tilde{g}(\tau) = \sigma \rho_1(\sigma)$. For simplicity, we want the expansion coefficients to be dimensionless. To fulfill this, we introduce dimensionless variables $s = \sigma/\Lambda^2 = 1/t$ and $u = Q^2/\Lambda^2$ in Eq. (3), where $\Lambda^2 = \Lambda_{\mathrm{QCD}}^2$ (in $\overline{\mathrm{MS}}$ convention; $\Lambda_{\mathrm{QCD}}^2 \sim 10^{-1}$ GeV^2). Consequently, Eqs. (9) and (10) obtain the form

$$\mathcal{A}_1^{(mMA)}(u\Lambda^2) = \frac{1}{\pi} \int_0^{1/s_0} dt \, \frac{g(t)}{1 + tu} = \sum_{n=0}^{\infty} L_n u^n, \tag{11}$$

with

$$L_n = \frac{(-1)^n}{\pi} \int_0^{1/s_0} t^n g(t) dt, \tag{12}$$

where $u = Q^2/\Lambda^2 = z/\Lambda^2$, $s_0 = M_0^2/\Lambda^2$, $L_n = \tilde{L}_n(\Lambda^2)^n$ are dimensionless, and $g(t) \equiv \rho_1(\Lambda^2/t)/t$.

An important consequence of the fact that $\mathcal{A}_1^{(mMA)}$ is a Stieltjes function is that the series in Eq. (9) only converges within the finite disc in the Q^2-plane ($Q^2 < M_0^2$), elsewhere the series is divergent. However, we will see that, because of the aforementioned theorem [3], only few coefficients of this divergent series are needed in order to evaluate $\mathcal{A}_1^{(mMA)}(Q^2)$ in regions well beyond the convergence disc, via approximate analytic continuation in the form of Padé approximants $R_M^{M-1}(z)$.

Following Ref. [4], we can approximate $\theta(s) \equiv g(t = 1/s) \equiv s\rho_1(\sigma = \Lambda^2 s)$ by a singular series expansion

$$\frac{s\rho_1(s\Lambda^2)}{\pi} \equiv \frac{g(1/s)}{\pi} \equiv \frac{\theta(s)}{\pi} \approx \sum_{n=1}^{M} f_n^2 s_n \delta(s - s_n) \, , \tag{13}$$

where $s = \sigma/\Lambda^2$, $s_n = M_n^2/\Lambda^2$ and f_n^2 are all positive dimensionless quantities. In Ref. [4], this type of approximation was applied to the spectral function of the vector channel vacuum polarization function $\Pi_V(Q^2)$. It was motivated there by the highly singular behavior of the vector spectral function in the limit $N_c \to \infty$. In our case we aren't working in that limit, but we note that the spectral function $\rho_1(\sigma)$ of $\mathcal{A}_1^{(mMA)}(Q^2)$ is positive; although $\theta(s)$ has finite values, such a function can be well approximated as a sum of positively weighted Dirac deltas for the purpose of integration. We will see that this approximation is equivalent to approximating the mMA coupling $\mathcal{A}_1^{(mMA)}(Q^2)$ as the Padé approximant $R_M^{M-1}(u)$.

Using the singular approximation (13) for $\theta(s)$ in Eq. (11), we obtain

$$\mathcal{A}_1^{(mMA)}(u\Lambda^2) \approx \sum_{n=1}^{M} \frac{f_n^2}{u + s_n} = \sum_{n=1}^{M} \frac{F_n^2}{Q^2 + M_n^2} \tag{14}$$

where $F_n^2 = f_n^2 \Lambda^2$. This relation is the same as $R_M^{M-1}(z)$ Padé of $\mathcal{A}_1^{(mMA)}$ given in Eq. (6), with $z = u$, $z_n = s_n$ and $d_n = f_n^2$

$$\mathcal{A}_1^{(mMA)}(u\Lambda^2) \approx R_M^{M-1}(u) = \sum_{n=1}^{M} \frac{f_n^2}{u + s_n} = \sum_{n=1}^{M} \frac{F_n^2}{Q^2 + M_n^2} \tag{15}$$

Therefore, by approximating $\theta(s)$ by positive Dirac deltas we obtain $\mathcal{A}_1^{(mMA)}$ written in a (paradiagonal) Padé form. Further, the following relation holds [3]:

$$|\mathcal{A}_1^{(mMA)}(u\Lambda^2) - R_M^{M-1}(u)| \leq K \left| \frac{\sqrt{s_0 + u} - \sqrt{s_0}}{\sqrt{s_0 + u} + \sqrt{s_0}} \right|^{2M}, \tag{16}$$

where K is a constant. Therefore $R_M^{M-1}(u) \to \mathcal{A}_1^{(mMA)}(u\Lambda^2)$ when $M \to \infty$.

In our evaluations we will use the perturbative coupling given by the solution of the two-loop renormalization group (RG) equation

$$a^{(2-\ell.)}(u\Lambda^2) = \frac{-1}{c_1(1 + W_{\mp 1}(z_\pm))}, \tag{17}$$

where $W_{\mp 1}(z)$ is the Lambert function (branches $n = \mp 1$), and the argument $z_\pm$ is given by

$$z_\pm = \left(\frac{|u|^{-\beta_0/c_1}}{c_1 e} \right) e^{i(\pm\pi - \phi\beta_0/c_1)}, \tag{18}$$

where $Q^2 = |Q^2|e^{i\phi}$, $|u| = |Q^2|/\Lambda^2$, $\beta_0 = (11 - 2n_f/3)/4$, $c_1 = \beta_1/\beta_0$, $\beta_1 = (102 - 38n_f/3)/16$. For $0 < \phi < \pi$, the branch $W_{-1}(z_+)$ is chosen, for $-\pi < \phi < 0$, the branch $W_{+1}(z_-)$ is chosen. At low energies ($|Q^2| \lesssim 10\ GeV^2$), the number of active quark flavors is $n_f = 3$. For details see Ref. [5]. With the coupling given in Eq. (17), the discontinuity function becomes

$$\rho_1^{(2-\ell.)}(s\Lambda^2) = \text{Im}\left[\frac{-1}{c_1(1 + W_{+1}(z_-(s)))} \right], \tag{19}$$

with $\phi = -\pi$ and $|u| = \sigma/\Lambda^2 \equiv s$ in Eq. (18). These expressions are in fact valid at any n-loop level ($n \geq 2$) in the 't Hooft renormalization scheme.
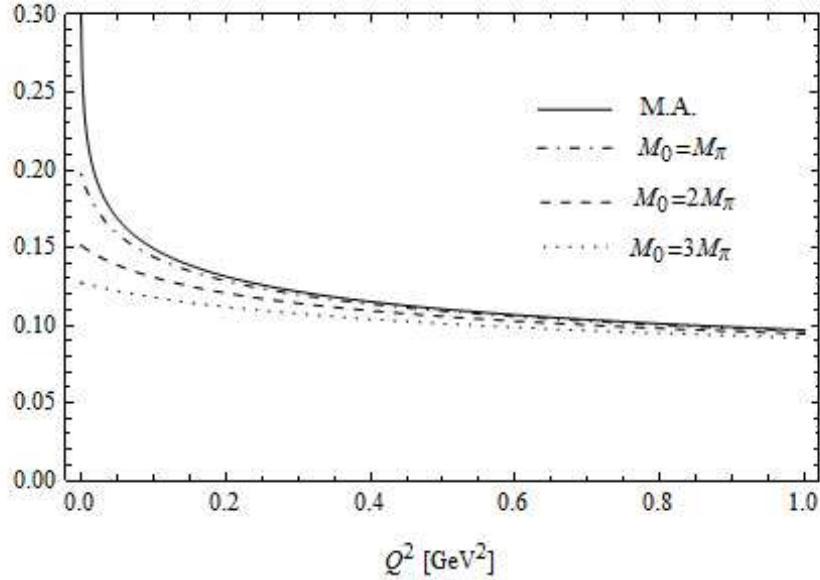

FIG. 1: $\mathcal{A}_1^{(MA)}(Q^2)$ (continuous), and $\mathcal{A}_1^{(mMA)}(Q^2)$ at two-loop level for various values of M_0 cut. Throughout this paper we use $n_f = 3$ and $\Lambda_{\overline{MS}} = 0.35$ GeV.

We set $\Lambda = 0.35$ GeV (at $n_f=3$).[2] This value can be changed later when we fit experimental data. Here we will compare numerically the accuracy of the rational approximants with the "exact" numbers, i.e., those obtained by evaluating numerically integrals Eq. (3).

[2] In Ref. [6], the value $\Lambda_{(n_f=3)} \approx 0.4$ GeV was obtained in MA by requiring that the MA model reproduce measured values of QCD observables at higher energies ($|Q| \gtrsim 10$ GeV) in $\overline{MS}$ scheme.
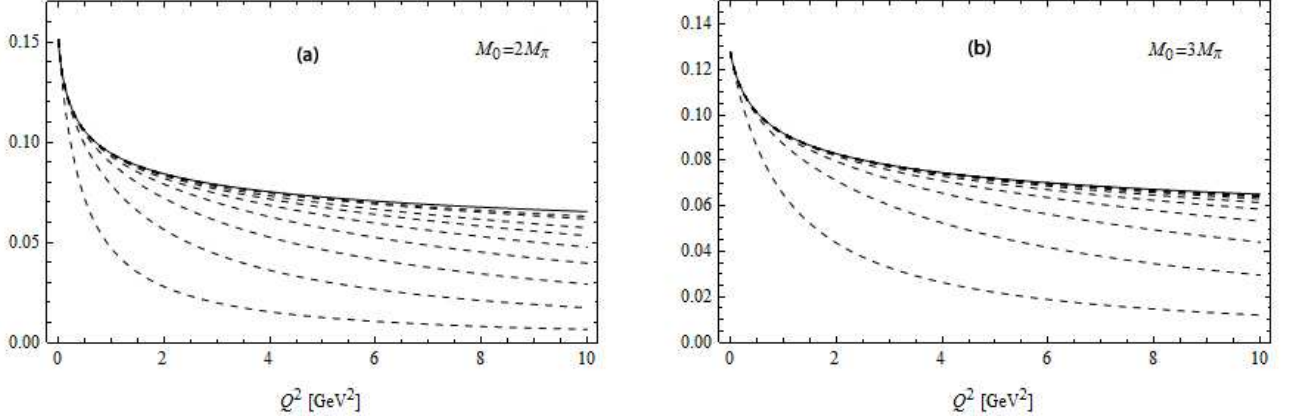
FIG. 2: The full line is the "exact" mMA coupling, Eq. (3). In both Figures, the dashed lines (starting from the bottom) are all Padé approximants R_M^{M-1}: R_1^0, R_2^1,..., R_{10}^9. The cut value M_0 is: (a) $M_0 = 2M_\pi$; (b) $M_0 = 3M_\pi$.

TABLE I: The first twenty coefficients computed with the discontinuity function at two-loop given in Eq. (19), for $M_0 = 2M_\pi$. In parentheses, the results for $M_0 = 3M_\pi$ are given. All the numbers here are presented as rounded off at the sixth digit.

L_n		L_n	
L_0	0.151418 (0.127410)	L_{10}	0.270477 ($6.95492 \cdot 10^{-5}$)
L_1	-0.0408795 (-0.0149290)	L_{11}	-0.384736 ($-4.40027 \cdot 10^{-5}$)
L_2	0.0353764 (0.00582799)	L_{12}	0.551687 ($2.80615 \cdot 10^{-5}$)
L_3	-0.0380741 (-0.00281121)	L_{13}	-0.796468 ($-1.80155 \cdot 10^{-5}$)
L_4	0.0453111 (0.00149464)	L_{14}	1.15653 ($1.16323 \cdot 10^{-5}$)
L_5	-0.0571406 ($-8.40628 \cdot 10^{-4}$)	L_{15}	-1.68780 ($-7.54792 \cdot 10^{-6}$)
L_6	0.0748244 ($4.90454 \cdot 10^{-4}$)	L_{16}	2.47387 ($4.91884 \cdot 10^{-6}$)
L_7	-0.100605 ($-2.93630 \cdot 10^{-4}$)	L_{17}	-3.63999 ($-3.21771 \cdot 10^{-6}$)
L_8	0.137943 ($1.79193 \cdot 10^{-4}$)	L_{18}	5.37405 ($2.11200 \cdot 10^{-6}$)
L_9	-0.192008 ($-1.10983 \cdot 10^{-4}$)	L_{19}	-7.95836 ($-1.39043 \cdot 10^{-6}$)

In Fig. 1 we compare mMA coupling (for various values of the IR cutoff M_0) with the standard MA coupling[3] at low positive Q^2's. These values are calculated by performing integrals in the dispersive relations (3) and (2) for each Q^2. An effect of increasing the value of the cutoff M_0^2 in Eq. (3) is to decrease the values of $\mathcal{A}_1^{(mMA)}(Q^2)$ at low Q^2.

We can compute L_n coefficients of mMA appearing in Eq. (11) by using the discontinuity function (19) in integrals (12). All the integrations are done numerically. The first twenty coefficients are shown in Table I. With these coefficients we can compute the paradiagonal Padé approximants $R_M^{M-1}(u)$ up to $R_{10}^9(u)$ (for higher Padé's we need more coefficients).

All the rational approximants $R_M^{M-1}(u)$ up to $R_{10}^9(u)$ for $\mathcal{A}_1^{(mMA)}(u\Lambda^2)$ are shown in the Figs. 2, for two choices of the IR cutoff in Eq. (3): $M_0 = 2M_\pi$, $3M_\pi$. We recall that M_0^2 is the convergence radius of the Stieltjes function $\mathcal{A}_1^{(mMA)}(Q^2)$. Since this radius is larger in Fig. 2(b), the convergence of the Padé approximants is also faster there. The rational function $R_{10}^9(Q^2)$ matches $\mathcal{A}_1^{(mMA)}(Q^2)$ in Fig. 2(a) quite well for all $0 < Q^2 < 10$ GeV^2, and in Fig. 2(b) the agreement is even better.

In order to give an idea of how the approximants work, we list in Table II the values of Q^2 at which the deviation from $\mathcal{A}_1^{(mMA)}(Q^2)$ reaches 0.1% (the deviation increases with increasing Q^2), for the case $M_0 = 2M_\pi$. For the Padé approximant $R_M^{M-1}(u)$ with $M = 10$ the deviation is less than 0.1% for all $Q^2 < 2.5$ GeV^2, and less than 1% for all $Q^2 \leq 5.4$ GeV^2 (when the Padé index is $M = 20$, these values increase to 10.33 GeV^2 and 22.63 GeV^2, respectively). We recall that these values are much higher than the convergence radius of the Taylor series, Eqs. (9) and (11): $R = Q^2 = M_0^2 = 0.0784$ GeV^2. We see that the first pole $(-s_1)$ converges from below to the IR cut

---

[3] $\mathcal{A}_1^{(MA)}(0) = 1/\beta_0 \approx 0.44$; however, the slope $d\mathcal{A}_1^{(MA)}(Q^2)/dQ^2$ at $Q^2 = 0$ is infinite.

TABLE II: The values of $Q^2 = u\Lambda^2$ at which the Padé approximants R_M^{M-1} (up to R_{10}^9), for $M_0 = 2M_\pi$, reach 0.1% deviation from $\mathcal{A}_1^{(mMA)}$. Further, the first few values $s_n \equiv M_n^2/\Lambda^2$ and f_n^2 are shown.

$R_M^{M-1}(u)$	Q^2 [GeV^2]	s_1	f_1^2	s_2	f_2^2	s_3	f_3^2
R_1^0	0.01	3.704	0.56085				
R_2^1	0.08	0.912073	0.0263116	13.2502	1.62407		
R_3^2	0.20	0.747835	0.00947914	1.62259	0.0538095	30.2372	3.19243
R_4^3	0.38	0.698643	0.00498205	1.04773	0.0185788	2.62744	0.0831117
R_5^4	0.60	0.677037	0.00309638	0.871413	0.00968867	1.46119	0.0275631
R_6^5	0.88	0.665567	0.00211868	0.7913	0.00604702	1.11052	0.0140762
R_7^6	1.20	0.658731	0.00154383	0.747386	0.00417231	0.951402	0.00869082
R_8^7	1.58	0.654321	0.00117625	0.720466	0.00306913	0.863709	0.00596662
R_9^8	2.02	0.651309	0.00092658	0.702677	0.00236037	0.809515	0.00438199
R_{10}^9	2.50	0.649158	0.000749085	0.690269	0.00187583	0.773381	0.0033713

$-s_0 = -M_0^2/\Lambda^2 = -4M_\pi^2/\Lambda^2$ ($-s_0 = -0.64$ in our case) when index M increases, as expected. For example, when $M = 10$, we obtain: $s_1 = 0.6492$ ($\approx s_0 = 0.6400$), $s_2 = 0.6907$, etc. When the cut M_0 is increased from $2M_\pi$ to $3M_\pi$ ($\Rightarrow -s_0 = -1.44$), we obtain for $M = 10$: $s_1 = 1.4605$ ($\approx s_0 = 1.44$), $s_2 = 1.5525$, etc.

IV. APPROXIMANTS FOR THE HIGHER POWER ANALOGS OF THE ANALYTIC COUPLING

To obtain the analogs of the higher powers of the analytic coupling in this formalism, we use relations given in Ref. [7]. At the 3-loop level truncated series for the analytic coupling, we have:

$$\mathcal{A}_2(Q^2) = \tilde{\mathcal{A}}_2(Q^2) - c_1 \tilde{\mathcal{A}}_3(Q^2), \qquad \mathcal{A}_3(Q^2) = \tilde{\mathcal{A}}_3(Q^2), \tag{20}$$

where

$$\tilde{\mathcal{A}}_n(Q^2) = \frac{(-1)^{n-1}}{\beta_0^{n-1}(n-1)!} \frac{\partial^{n-1}\mathcal{A}_1(Q^2)}{\partial(\ln Q^2)^{n-1}}. \tag{21}$$

The correspondence between the powers a^k of the perturbative coupling $a(Q^2) = \alpha_s(Q^2)/\pi$ and the above quantities is: $a^k \mapsto \mathcal{A}_k$. The couplings $\mathcal{A}_k$ are the analytic versions ("analogs") of higher powers needed for evaluation of observables. We note that in general $\mathcal{A}_k \neq \mathcal{A}_1^k$ (for further discussion, c.f. Sec. III of Ref. [7]).

Using the dispersive integral expression Eq. (3) in Eqs. (21), we obtain explicit expressions for $\mathcal{A}_k$'s in terms of integrals of the (perturbative) discontinuity function ρ_1

$$\mathcal{A}_2^{(mMA)}(u\Lambda^2) = \frac{u}{\beta_0\pi} \int_{s_0}^\infty \frac{\rho_1(s\Lambda^2)}{(s+u)^2} ds - c_1 \mathcal{A}_3^{(mMA)}(u\Lambda^2), \tag{22}$$

$$\mathcal{A}_3^{(mMA)}(u\Lambda^2) = \frac{-u}{2\beta_0^2\pi} \int_{s_0}^\infty \frac{\rho_1(s\Lambda^2)(s-u)}{(s+u)^3} ds. \tag{23}$$

We see from here that the quantities $\mathcal{A}_k^{(mMA)}(Q^2)$ have the same location of the singularities as $\mathcal{A}_1^{(mMA)}$: $Q^2 < -M_0^2$ ($= -\Lambda^2 s_0$). On the other hand, the poles $Q^2 = -M_n^2 = -s_n\Lambda^2$ ($n = 1, \ldots, M$) of the Padé approximants R_M^{M-1} for $\mathcal{A}_1$, Eq. (15), do reflect, in a discretized manner, the singularity cut of $\mathcal{A}_1^{(mMA)}$; namely, these poles appear on the negative real axis in the range: $-\infty < -M_M^2 < -M_{M-1}^2 < \cdots < -M_1^2$ ($< M_0^2$). Such a pole structure of $R_M^{M-1}(u)$ is guaranteed because $\mathcal{A}_1^{(mMA)}$ is a Stieltjes function [3]. On the other hand, the analytic higher power analogs $\mathcal{A}_k^{(mMA)}(Q^2)$ ($k \geq 2$) are no longer Stieltjes functions. Therefore, if we construct the Padé approximants $R_M^{M-1}(u)$ for $\mathcal{A}_k^{(mMA)}(Q^2)$ ($k \geq 2$) in the usual way, i.e., based on the first $2M$ coefficients of their Taylor expansion around $Q^2 = 0$, there is no longer the guarantee that all the poles of the obtained rational functios lie on the negative real axis (and below $-M_0^2$). For instance, the Padé approximant R_{10}^9 computed from the series of $\mathcal{A}_3$ has a non-physical pole on the positive real axis. One way to avoid this problem is to compute the rational approximants of $\mathcal{A}_k$'s directly from the derivatives of the Padé approximant of $\mathcal{A}_1^{(mMA)}$. If $R_M^{M-1}(u)$ are the paradiagonal Padés that approximate $\mathcal{A}_1^{(mMA)}(u\Lambda^2)$, we shall define the rational approximants $R_2(u)$ and $R_3(u)$ for $\mathcal{A}_2^{(mMA)}(u\Lambda^2)$ and $\mathcal{A}_3^{(mMA)}(u\Lambda^2)$,

respectively, in the following way:

$$R_2(u) = \tilde{R}_2(u) - c_1 \tilde{R}_3(u), \qquad R_3(u) = \tilde{R}_3(u), \tag{24}$$

where

$$\tilde{R}_n(u) = \frac{(-1)^{n-1}}{\beta_0^{n-1}(n-1)!} \frac{\partial^{n-1} R_M^{M-1}(u)}{\partial(\ln u)^{n-1}}. \tag{25}$$

A comparison between R_k and their respective $\mathcal{A}_k$, computed from $R_{10}^9(u)$ (i.e., Padé index $M = 10$), is shown in
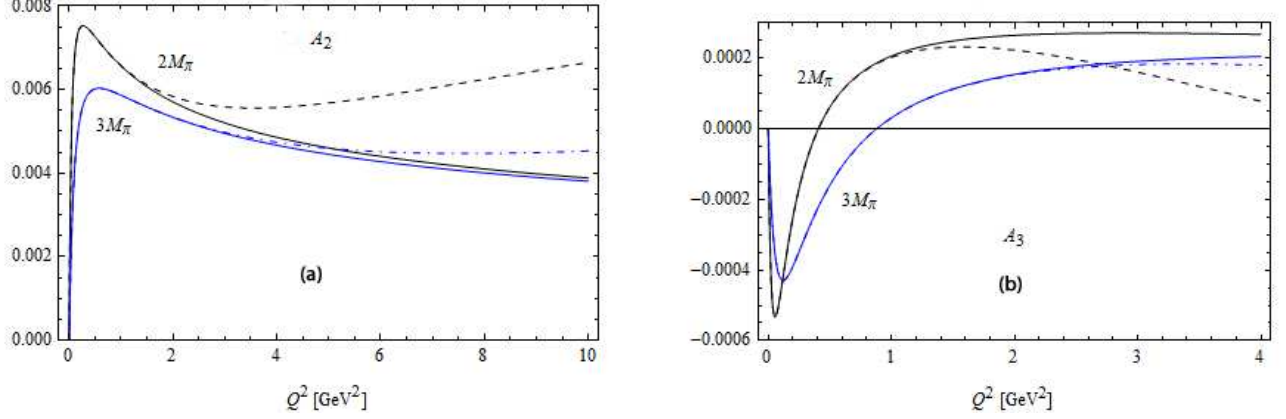

FIG. 3: Comparison between: (a) $\mathcal{A}_2^{(mMA)}$ (continuous) and R_2 (dashed and dot-dashed), for two choices of IR cut $M_0 = 2M_\pi$ and $M_0 = 3M_\pi$, respectively; (b) the same as in (a), but now for $\mathcal{A}_3^{(mMA)}$ and R_3. Padé index is $M = 10$.

Figs. 3. The accuracy of these approximants decreases notably compared to the R_M^{M-1} approximants of $\mathcal{A}_1^{(mMA)}$. The accuracy of the approximants increases when the cut M_0 increases, e.g., from $2M_\pi$ to $3M_\pi$.

V. COMPLEX ARGUMENTS

In evaluation of observables, sometimes evaluation of the analytic coupling and their power analogs at complex values of arguments is needed (e.g., see App. C of Ref. [7]). For some complex arguments $Q^2 = |Q^2| \exp(i\phi)$ [$u \equiv Q^2/\Lambda^2 = |u| \exp(i\phi)$], the results based on the approximant $R_{10}^9(u)$ (Padé index $M = 10$), are shown in Figs. 4-7. When $\phi = \pi/4$, Figs. 4 (a), (b) show that the approximant for $\mathcal{A}_1^{(mMA)}(Q^2)$ works with less than 1% error up to $|Q^2| \approx 10$ GeV^2 for the real part, and $|Q^2| \approx 3$ GeV^2 for the imaginary part. The approximants $R_2(u)$ and $R_3(u)$ for $\mathcal{A}_2$ and $\mathcal{A}_3$, (see Figs. 6-7) fail already at lower $|Q^2|$. Figs. 5 (a), (b) show the approximant for $\mathcal{A}_1^{(mMA)}(Q^2)$ when $\phi = 3\pi/4$. Figs. 4-7 indicate that the relative accuracy of our approximants decreases: (I) when the index n of the power analog $\mathcal{A}_n$ increases; (II) when the considered ray $Q^2 = |Q^2| \exp(i\phi)$ comes closer to the time-like semiaxis ($|\phi|$ closer to π). Aspect (I) can be understood from the fact that, by our construction, R_n involves $(n-1)$ derivatives of the Padé approximant $R_1 \equiv R_M^{M-1}$. Aspect (II) is also to be expected, because rays with $\phi \approx \pm\pi$ are close to the singularity cut of $\mathcal{A}_n$'s.

The accuracy can be increased if we compute $R_1 \equiv R_M^{M-1}$ as a higher order Padé (higher index M). For instance, Figs. 8 (a), (b) show the approximants for $\mathcal{A}_2^{(mMA)}$, with $\phi = \pi/4$, which are calculated from $R_{20}^{19}(u)$ (i.e., Padé index $M = 20$). The latter is calculated from the first 40 coefficients of the Taylor series of $\mathcal{A}_1^{(mMA)}(u\Lambda^2)$. We see that in the case of $M_0 = 2M_\pi$, the deviation of Re$[R_2]$ from Re$[\mathcal{A}_2]$ becomes discernible to the eye (1% deviation) only for $Q^2 > 5$ GeV^2; this is to be compared with Fig. 6 (a) (where Padé index $M = 10$). If we used $\phi = 0$ instead (see Figs. 3 where $M = 10$), the deviations of Re$[R_2]$ from Re$[\mathcal{A}_2]$, for $M = 20$ and $M_0 = 2M_\pi$, on the scale of Figs. 8 would turn out to be discernible to the eye only for $Q^2 > 6$ GeV^2, i.e., the convergence turns out to be even better than in the case $\phi = \pi/4$. The deviations of Im$[R_2]$ from Im$[\mathcal{A}_2]$ in Fig. 8 (b) are not discernible to the eye. We also see that the deviations of R_2 from $\mathcal{A}_2$ cannot be seen by the eye in Figs. 8 when the cut value M_0 increases to $3M_\pi$.[4]

---

[4] At the level $M = 20$, it is important that the 40 Taylor coefficients L_n and the coefficients of the Padé approximant R_M^{M-1} be calculated

Both aforementioned aspects (I, II) that decrease accuracy are, however, not very important in practice when evaluating observables. Namely, the higher order contributions ($\sim \mathcal{A}_n$) are very suppressed in anQCD (even when $|Q^2|$ is low), and the contributions of Q^2 near the time-like axis in the contour-type of integrations (e.g., for the semihadronic τ decay ratio r_τ) are usually suppressed by the integrand.
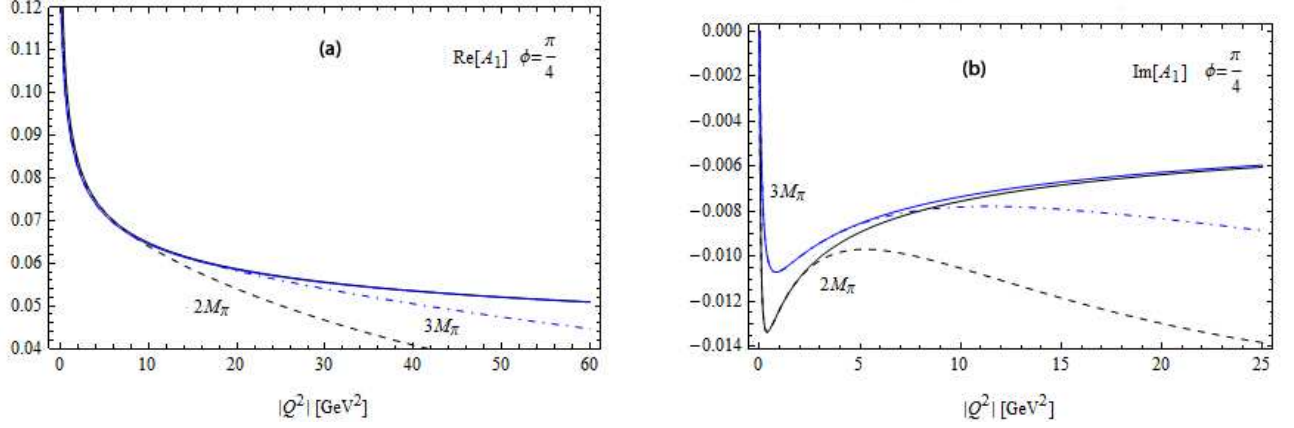

FIG. 4: (a) Real parts of $\mathcal{A}_1^{(mMA)}$ and R_{10}^9 with complex arguments $Q^2 = |Q^2|\exp(i\pi/4)$; (b) same as in (a), but for imaginary parts.
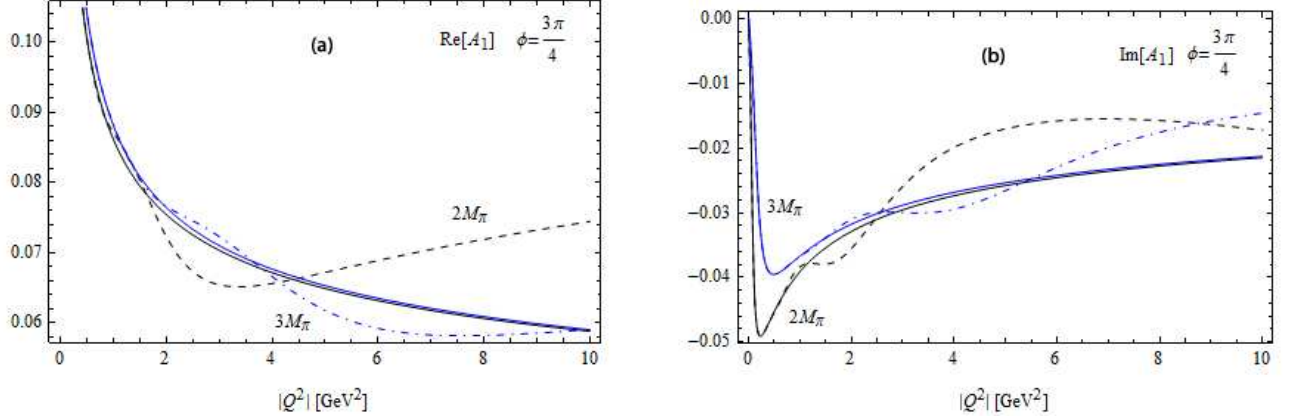

FIG. 5: (a) Real parts of $\mathcal{A}_1^{(mMA)}$ and R_{10}^9 with complex arguments $Q^2 = |Q^2|\exp(i3\pi/4)$; (b) same as in (a), but for imaginary parts.

VI. PROSPECTS OF APPLICATIONS IN FITTING EXPERIMENTAL DATA

In Eq. (3) we considered the dispersive relation for $\mathcal{A}_1$ with an IR σ-cutoff $\sigma_{\rm cut} = M_0^2$ ($\sim M_\pi^2$) imposed on the perturbative QCD discontonuity function $\rho_1(\sigma) \equiv {\rm Im}[a(Q^2 = -\sigma - i\epsilon)]$. Such a cutoff results in the analyticity of $\mathcal{A}_1$ around $Q^2 = 0$, thus reflecting the analyticity of space-like observables $\mathcal{D}(Q^2)$ in the complex plane excluding the time-like semiaxis but including a regime around $Q^2 = 0$.

---

to high accuracy (to at least about 20 and 30 digits, respectively), in order to avoid numerical instabilities connected with cancellation of large numbers.
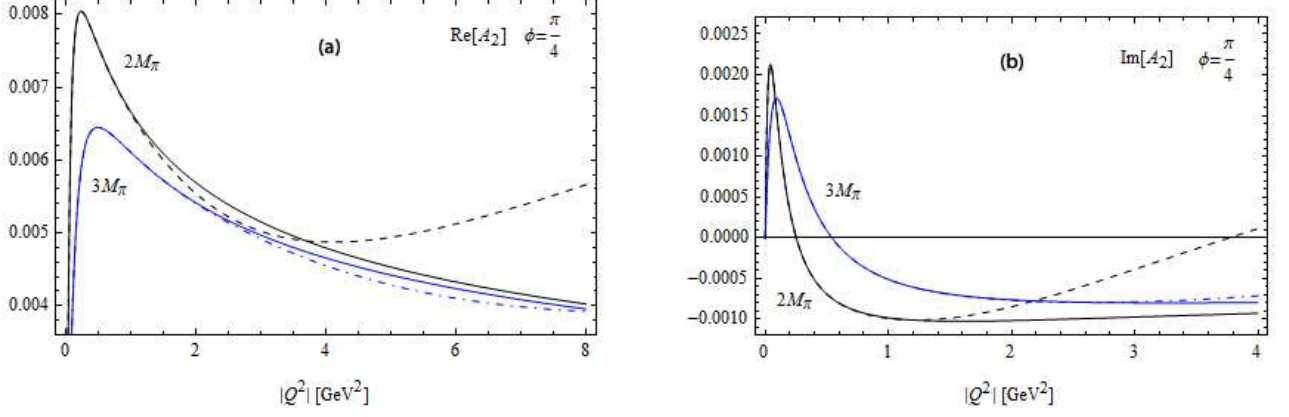
FIG. 6: (a) Real parts of $\mathcal{A}_2^{(mMA)}$ and R_2 with complex arguments $Q^2 = |Q^2| \exp(i\pi/4)$; (b) same as in (a), but for imaginary parts.
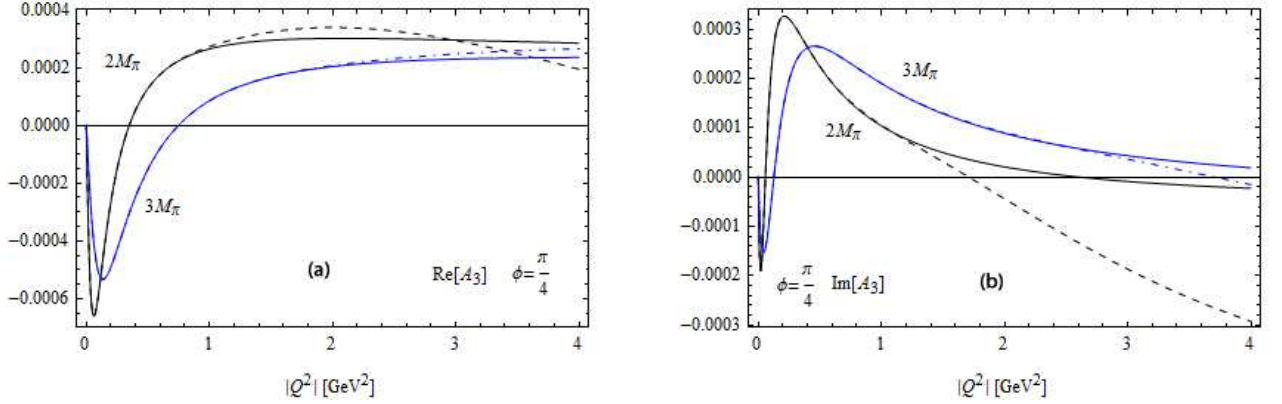

FIG. 7: (a) Real parts of $\mathcal{A}_3^{(mMA)}$ and R_3 with complex arguments $Q^2 = |Q^2| \exp(i\pi/4)$; (b) same as in (a), but for imaginary parts.

In MA model, the scale Λ can be fixed so that it reproduces measured values of QCD observables at higher energies $Q \gtrsim 10$ GeV ($\Rightarrow \Lambda_{n_f=3} \approx 0.4$ GeV) [6]. However, then MA gives too low value of the massless strangeless ($\triangle S = 0$) semihadronic τ-decay ratio: $r_\tau \approx 0.14$ [7, 8]. The experimentally measured value of this quantity is: $r_\tau = 0.204 \pm 0.005$ [9]. The latter value can be reproduced in MA with $\Lambda_{(n_f=3)} \approx 0.4$ GeV only if the current masses of light quarks ($m_u, m_d \sim 1$ MeV) are replaced by much larger (constituent) masses ($m_u, m_d \approx 0.25$ GeV) [10] and the threshold effects become very important.

By introducing IR cutoff $\sigma_{\text{cut}} = M_0^2$, the coupling $\mathcal{A}_1$ gets further diminished at low Q^2, and thus further diminishes the value of r_τ. To remedy this situation, we can, in the simplest way, simulate the unknown behavior of $\rho_1(\sigma)$ (Fig. 9) at $\sigma \lesssim M_0^2$ by adding a simple positive Dirac delta peak: $\delta\rho_1(s\Lambda^2) = \pi f_{-1}^2 \delta(s - s_{-1})$, where $0 < s_{-1} \lesssim s_0 (\equiv M_0^2/\Lambda^2)$. This would then allow us to achieve, in the model, the correct value of r_τ while still maintaining the analyticity of $\mathcal{A}_1$ around $Q^2 = 0$. Thus, the full discontinuity function in such a "delta-modified" MA model (dmMA) is

$$\rho_1^{(\text{dmMA})}(s\Lambda^2) = \Theta(s - s_0)\rho_1(s\Lambda^2) + \pi f_{-1}^2 \delta(s - s_{-1}) , \tag{26}$$

where $\Theta(x)$ is the Heaviside step function ($+1$ for $x > 0$, zero otherwise), and $\rho_1(s\Lambda^2)$ is the pertubative QCD discontinuity function: $\rho_1(s\Lambda^2) = a(-s\Lambda^2 - i\epsilon)$. This leads to the following $\mathcal{A}_1$:

$$\mathcal{A}_1^{(dmMA)}(u\Lambda^2) = \frac{1}{\pi} \int_{s_0}^{\infty} ds \frac{\rho_1(s\Lambda^2)}{s + u} + \frac{f_{-1}^2}{u + s_{-1}} . \tag{27}$$
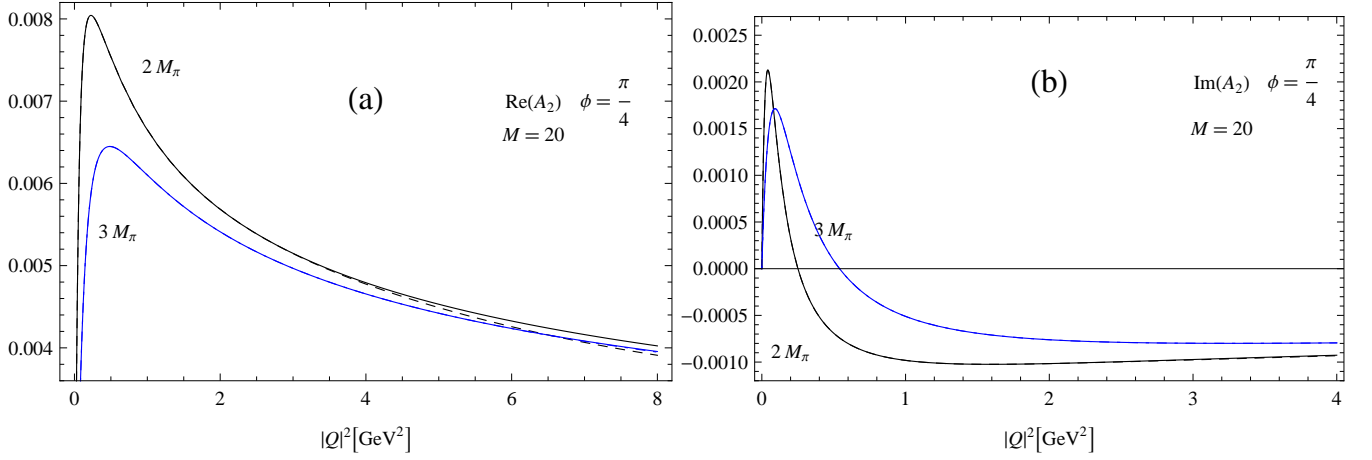
FIG. 8: Now R_2 is computed from the Padé R_{20}^{19} of $\mathcal{A}_1^{(mMA)}$ ($M = 20$): (a) real parts of $\mathcal{A}_2^{(mMA)}$ (continuous) and R_2 (dashed and dot-dashed), for the IR cut value $M_0 = 2M_\pi$, $3M_\pi$, respectively, with complex arguments $Q^2 = |Q^2| \exp(i\pi/4)$; (b) same as in (a), but for imaginary parts. For $M_0 = 3M_\pi$, no deviations of R_2 from $\mathcal{A}_2^{(mMA)}$ can be seen by the eye.

Applying the Padé $R_M^{M-1}(u)$ approximation to this analytic coupling we obtain

$$\mathcal{A}_1^{(\mathrm{dmMA})}(u\Lambda^2) \approx R_M^{M-1}(u) = \sum_{n=-1(n\neq 0)}^{M} \frac{f_n^2}{u + s_n} = \sum_{n=-1(n\neq 0)}^{M} \frac{F_n^2}{Q^2 + M_n^2} \,. \tag{28}$$

This has the same form as the Padé $R_M^{M-1}(u)$ applied to $\mathcal{A}_1^{(\mathrm{mMA})}$ (MA with IR cut), Eq. (15), but just with one more term ($n = -1$). This model has three dimensionless model parameters: s_0, s_{-1}, f_{-1}. All are positive and ~ 1. As presented, the model is considered in the 't Hooft scheme ($\beta_j = 0$ for all $j \geq 2$). The scale parameter $\Lambda_{n_f=3}$ is fixed by fitting the model to experimental values of observables at high energies ($|Q| \gtrsim 10$ GeV), such as Υ decay, $e^+e^- \to$ hadrons, $Z \to$ hadrons. The values of low energy QCD observables ($|Q| \sim 1$ GeV), such as r_τ and Bjorken polarized sum rule, are sensitive to the values of parameters s_0, s_{-1} and f_{-1}; therefore, the latter are to be fixed by fitting to the experimental values of such observables.
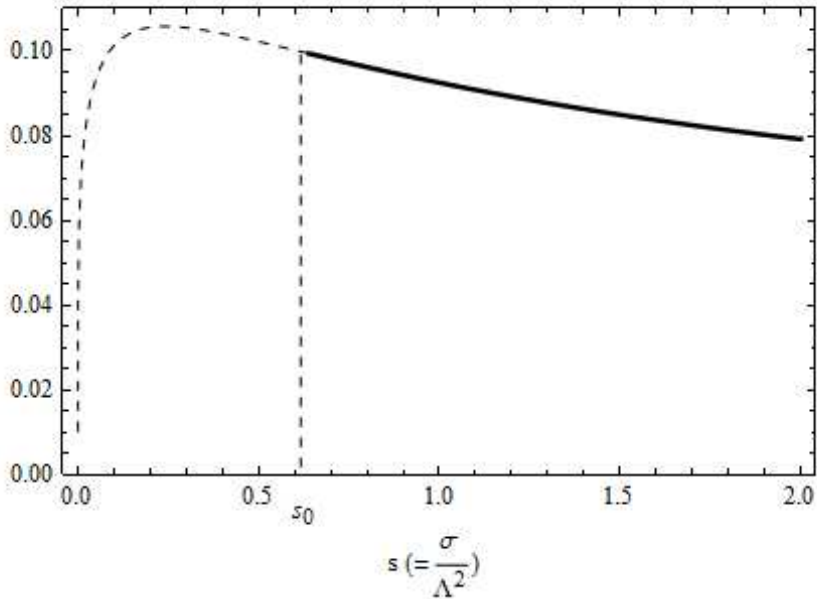

FIG. 9: This Figure shows the IR cut $s_0 = M_0^2/\Lambda^2$ (when $M_0 = 2M_\pi$) for perturbative ρ_1 that was used starting in Eq. (3). The unknown low momentum part ($0 < s \lesssim s_0$) can be simulated by adding a Dirac delta, say $\pi f_{-1}^2 \delta(s - s_{-1})$, where $0 < s_{-1} \lesssim s_0$.

We see that even with this modification (dmMA) of the MA, the evaluation of the couplings $\mathcal{A}_n(u\Lambda^2)$ ($n = 1, 2, \ldots$) is made simple and efficient by using the Padé approximant (28); for the evaluation, it suffices to know the (three) parameters s_0, s_{-1} and f_{-1} and the first few coefficients L_k [Eqs. (11)-(12) and Table I].

VII. SUMMARY

We worked with the minimal analytic (MA) model modified (mMA) by an IR cutoff $\sigma_{\text{cut}} = M_0^2 \sim M_\pi^2$ for the perturbative discontinuity function. In such a model, the analytic coupling $\mathcal{A}_1(Q^2)$ is analytic in the entire Q^2-complex plane excluding the semi-axis $Q^2 < -M_0^2$. The analytic properties of such (mMA) coupling reflect the analytic properties of space-like QCD observables $\mathcal{D}(Q^2)$, among them analyticity in the point $Q^2 = 0$ and its vicinity. Further, such a (mMA) coupling is a Stieltjes function of Q^2. This implies that it will be efficiently approximated by (paradiagonal) Padé approximants $R_M^{M-1}(Q^2)$, i.e., $R_M^{M-1}(Q^2)$ converges to $\mathcal{A}_1(Q^2)$ at any point of analyticity when index M increases ($M \to \infty$). The coupling $\mathcal{A}_1(Q^2)$ in the form of $R_M^{M-1}(Q^2)$ can be easily and efficienty evaluated [i.e., without performing time-consuming dispersion-type integrations (3) for each Q^2] just by knowing the first few coefficients of Taylor expansion of $\mathcal{A}_1(Q^2)$ in powers of Q^2.

We showed that for real and complex arguments the paradiagonal Padé approximants of the analytic coupling $\mathcal{A}_1^{(mMA)}(Q^2)$ are precise at low positive Q^2's. This high precision range of positive Q^2's increases fast when the order index M of the Padé approximant increases. When Q^2's are complex, the precision range of $|Q^2|$'s decreases when Q^2 approaches the singularity cut. The analytic analogs $\mathcal{A}_n^{(mMA)}$ of higher powers $a^n = (\alpha_s/\pi)^n$ ($n \geq 2$) are then evaluated as combinations of logarithmic derivatives of the approximant $R_M^{M-1}(Q^2)$ [$\approx \mathcal{A}_1(Q^2)$]. The approximants obtained in this way for $\mathcal{A}_n^{(mMA)}$ show less precision when n increases and/or when Q^2 approaches the singularity cut. These approximants still work fine if we increase the order index M of the Padé. However, high precision is needed only for the $n = 1$ case, because the higher couplings $\mathcal{A}_n^{(mMA)}$ get strongly suppressed (even at low $|Q^2|$) in analytic QCD when n increases. Further, when evaluation of observable involves contour integration (such as, for example, in the case of r_τ), the contributions of $\mathcal{A}_n(Q^2)$ get supressed by the rest of the integrand when Q^2 comes close to the singularity cut. While we generally used for the IR cutoff σ_{cut} ($\sim M_\pi^2$) the specific value $\sigma_{\text{cut}} (\equiv M_0^2) = 4M_\pi^2$, we also showed that the conclusions in this work are independent of the specific value chosen, by comparing various results for $M_0 = 2M_\pi$ and $M_0 = 3M_\pi$.

We further suggested an inclusion of one additional Dirac delta function to the mMA discontinuity function $\theta(\sigma - M_0^2)\rho_1(\sigma)$ at low energies where the precise behavior of ρ_1 is unknown - Dirac modified MA model (dmMA). Such a modification maintains the analyticity at $Q^2 = 0$ and its vicinity, and allows us to reproduce the experimental value of the semihadronic τ decay ratio r_τ. Such a modification keeps the same form of the Padé approximants $R_M^{M-1}(Q^2)$ of $\mathcal{A}_1^{(dmMA)}$ as in the mMA case and allows us to evaluate them (and the higher power analogs) in an easy and efficient manner. The (three) parameters of such a model can be determined by requiring that the model reproduces the measured values of low energy QCD observables [11].

[1] D. V. Shirkov and I. L. Solovtsov, hep-ph/9604363; Phys. Rev. Lett. **79**, 1209 (1997) [hep-ph/9704333].
[2] A. V. Nesterenko and J. Papavassiliou, Phys. Rev. D **71**, 016009 (2005) [hep-ph/0410406]; Nucl. Phys. Proc. Suppl. **164**, 304 (2007) [arXiv:hep-ph/0507320].
[3] G. A. Baker and P. Graves-Morris, *Padé Approximants*, Encyclopedia of Mathematics and its Applications (Cambridge University, Cambridge, England, 1996).
[4] S. Peris, Phys. Rev. D **74**, 054013 (2006) [arXiv:hep-ph/0603190].
[5] E. Gardi, G. Grunberg and M. Karliner, JHEP **9807**, 007 (1998) [arXiv:hep-ph/9806462].
[6] D. V. Shirkov, Theor. Math. Phys. **127**, 409 (2001) [hep-ph/0012283]; Eur. Phys. J. C **22**, 331 (2001) [hep-ph/0107282].
[7] G. Cvetič and C. Valenzuela, Phys. Rev. D **74**, 114030 (2006) [arXiv:hep-ph/0608256].
[8] K. A. Milton, I. L. Solovtsov, O. P. Solovtsova and V. I. Yasnov, Eur. Phys. J. C **14**, 495 (2000) [hep-ph/0003030].
[9] R. Barate *et al.* [ALEPH Collaboration], Eur. Phys. J. C **4**, 409 (1998); K. Ackerstaff *et al.* [OPAL Collaboration], Eur. Phys. J. C **7**, 571 (1999) [hep-ex/9808019]; S. Schael *et al.* [ALEPH Collaboration], Phys. Rept. **421**, 191 (2005) [hep-ex/0506072]; M. Davier, A. Höcker and Z. Zhang, hep-ph/0507078.

[10] K. A. Milton, I. L. Solovtsov, O. P. Solovtsova, Phys. Rev. D **64**, 016005 (2001) [hep-ph/0102254]; Mod. Phys. Lett. A **21**, 1355 (2006) [hep-ph/0512209].

[11] G. Cvetič and H. E. Martínez, work in progress.